A New Universal Approach to Modeling and Simulation of UWB Channels Containing Convex Obstacles Using Spice-Like Programs

Piotr Gorniak[1], Wojciech Bandurski[2]
[1] (Affiliation): dept. of Electronics and Telecommunications, Poznan University of Technology, Poznan, Poland, e-mail: pgorniak@et.put.poznan.pl
[2] (Affiliation): dept. of Electronics and Telecommunications, Poznan University of Technology, Poznan, Poland

***Abstract*— The paper presents a new approach to time domain modeling of UWB channels with elliptical shape convex obstacles. Rational approximation exploiting the vector fitting algorithm (VF) is used for deriving the closed form impulse response of a diffraction ray creeping on a convex obstacle. The VF algorithm is performed with respect to new generalized variables proportional to frequency but also taking into account geometrical parameters of the obstacles. Obtained impulse response is a sum of exponential functions. As a consequence, in simulations of electromagnetic (EM) wave propagation we can perform simulations implementing SPICE-like programs.**

***Index Terms*—ultra-wideband, vector fitting, time domain, conducting cylinder, uniform theory of diffraction.**

I. INTRODUCTION

Ultra-wideband (UWB) technology enables many beneficial possibilities in data transmission and radar area [1]. In order to take advantage of these possibilities, careful analysis of a given UWB system is required, in particular analysis of the propagation channel.

We focus our considerations on effective time domain modeling of UWB channels that comprise obstacles (e.g. people) which can be modeled by convex objects (cylinders in the 3D case or ovals in the 2D case). The EM wave hitting an obstacle can be reflected, diffracted or it can pass through this obstacle. Our aim is to present the method for obtaining a simple, closed form impulse response which can mathematically describe such phenomena. For the sake of clarity and simplicity of the description of this approach we consider the diffraction case only. We use the Uniform Theory of Diffraction (UTD) in our analysis. In the paper we give a simple, closed form impulse response for the creeping ray, as well as the procedure for obtaining it.

The analytical description of the propagation of the EM wave on convex objects in the time and the frequency domain was already considered in the literature, e.g. [2, 3]. The disadvantage of these solutions is their high complexity which can result in very long time of computation when especially multiple obstacles are considered.

In this paper, we introduce a universal rational approximation, valid for cases of diffraction rays creeping along short as well as long distances [4, 5] and independent of geometry of the objects in the cascade, and of the frequency band. For this purpose, we introduce new variables for which we carry out universal rational function approximation by means of the VF algorithm [6]. These new variables depend on the frequency and the geometry of a diffraction scenario. Using this approach we have to perform the rational approximation once. The obtained coefficients can be then used in many other scenarios and frequency ranges. In this way we obtain a universal approximation of the transfer function of the channel containing convex object that can be used for all considered scenario geometries and frequency bands (of course in reasonable limits).

The rest of the paper is organized as follows. In Section 2 we revise the concept of the UTD transfer function for a creeping ray. In section 3 we describe the procedure of obtaining the closed form universal rational approximation of the transfer function of a creeping ray. Simulation of the channel consisting a convex object in a SPICE simulator is shown in Section 4. In section 5 some examples are given. Section 6 concludes the paper.

II. THE UTD CREEPING RAY UNIVERSAL TRANSFER FUNCTION

The case of one diffraction ray that creeps on a convex obstacle in the form of elliptical 2D conducting cylinder is shown in Fig. 1. The transmitting and receiving antennas are placed at points Ta and Ra, respectively. The attachment and shedding points are marked with Q' and Q, respectively. The main parameters of the scenario are: a and b – the axes of the elliptical cylinder, γ' and γ – the parametrical coordinates of the points Q'and Q, respectively. The distances along which the EM wave propagates in the air are denoted by s_0 and s_1. Fourier transforms of the electric field at the output of the transmitting antenna – $E^{Ta}(\omega)$ and at the input of the receiving antenna – $E^{Ra}(\omega)$ for one creeping ray (Fig.1) are related by the expression:

$$E^{Ra}(\omega) = E^{Ta}(\omega) \cdot H_A(\omega) \cdot exp\left(-j \cdot \frac{\omega}{V_0} \cdot s^p\right) \times A^c(s_0, s_1)\,, \quad (1)$$

where s_p is the total length of the creeping ray, v_o is the speed of EM wave in free space, $A_c(s_0,s_1)$ is the spreading factor [7] and $H_A(\omega)$ is the transfer function of a creeping ray.

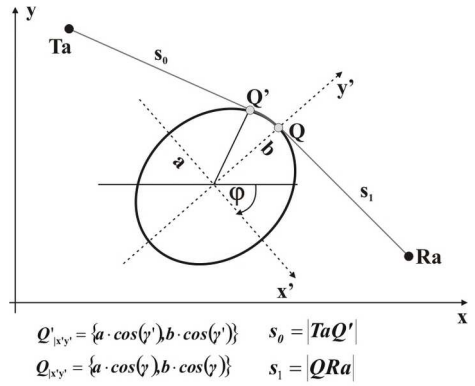

Fig. 1. The scenario of a diffraction ray creeping on a elliptical 2D cylinder.

The transfer function $H_A(\omega)$ can be presented as follows [8]:

$$H_A(\omega) = H_{A1}(\omega) + H_{A2}(\omega)\,, \tag{2}$$

where:

$$H_{A1}(\omega) = AmpAT \cdot exp\left(-j\frac{\pi}{4}\right)\frac{F_T(X_d)}{\sqrt{X_d}}, \tag{3}$$

$$AmpAT = \sqrt{\frac{L_d}{4\pi}}, \tag{4}$$

$$L_d = \frac{s_0 s_1}{s_0 + s_1}, \tag{5}$$

$$X_d = \frac{\omega L_d \theta^2}{2V_0}, \tag{6}$$

$$\theta = abF_c\sqrt{T_c}\,, \tag{7}$$

$$T_c = \frac{1}{\sqrt{[a\cdot sin(\gamma')]^2+[b\cdot cos(\gamma')]^2}} \times \frac{1}{\sqrt{[a\cdot sin(\gamma)]^2+[b\cdot cos(\gamma)]^2}}\,, \tag{8}$$

$$F_c = \left|\int_{\gamma_r}^{\gamma} \frac{1}{\sqrt{[a\cdot sin(\gamma)]^2 + [b\cdot cos(\gamma)]^2}}\right| d\gamma\,, \tag{9}$$

and

$$H_{A2}(\omega) = AmpAF \times \left[-exp\left(-j\frac{\pi}{4}\right)\frac{\begin{matrix}p^*(\xi_d)\\ q^*(\xi_d)\end{matrix}}{\sqrt{\xi_d}}\right], \tag{10}$$

$$AmpAF = \sqrt{\frac{F_c}{T_c}}, \tag{11}$$

$$\xi_d = \left(\frac{\omega \cdot R_{el}}{2V_0}\right)^{1/3} \cdot \theta_{el}\,, \tag{12}$$

$$R_{el} = \left(\frac{1}{\sqrt{T_c}}\right)^3 \cdot \frac{1}{ab}. \tag{13}$$

$F_T(X_{d(n)})$ in (3) is the transition function [7], while $p^*(\xi_d)$ and $q^*(\xi_d)$ are Fock scattering functions for the TM and the TE polarisation case, respectively [7].

In order to find the universal VF approximation of (2) dedicated to general, practical UWB scenarios, we rearrange $H_A(\omega)$ into a function of variables X_d and a new variable ξ_{dsub}, which is given by:

$$\xi_{dsub} = \frac{\omega \cdot {R_{el}}^2}{2V_0} \cdot {\theta_{el}}^3\,. \tag{14}$$

Now the components of (2) obtain the following form:

$$H_{A1}(X_d) = AmpAT \times exp\left(-j\frac{\pi}{4}\right)\frac{F_T(X_d)}{\sqrt{X_d}} = AmpAT \cdot V_{T1}(X_d)\,, \tag{15}$$

$$H_{A2}(\xi_{dsub}) = AmpAF \cdot \left[-exp\left(-j\frac{\pi}{4}\right)\frac{p^*\left({\xi_{dsub}}^{1/3}\right)}{\sqrt{{\xi_{dsub}}^{1/3}}}\right] = AmpAF \cdot V_{F1}(\xi_{dsub})\,. \tag{16}$$

For the sake of clarity and simplicity of further considerations we choose only one polarization of the EM wave. Therefore we assume that the electric field of the propagating wave is tangential to the cylinders. Consequently we use only $p^*(\xi_d)$ in (10) and in the rest of the paper.

III. VF APPROXIMATION

Equations (3) and (10), define the components of function $H_A(X_d, \xi_{dsub})$. There are two functions of different arguments: $V_{T1}(X_d)$, $V_{F1}(\xi_{dsub})$, which are to be approximated with VF. In order to apply VF approximation we must determine the ranges of variables X_d and ξ_{dsub}. These ranges should reflect the values of the UWB channel parameters that can be met in a real scenario.

We focus on convex objects which may model humans in an UWB channel. These objects can be cylinders with circular or ellipsoidal cross section with parameter R_{el} (13) in the range $0.2 \le R_{el} \le 0.3$ [m] - compare [9]. The remaining parameters whose ranges must be found are frequency f, parameter θ_{el} (7) and the separation coefficient L_d (5). We assume that $0.5 \le f \le 10$ [GHz] (typical UWB spectrum), $10^{-4} \le \theta_{el} \le \pi$ [rad] and that separation coefficient L_d is in the range 0.5 – 5 [m].

With the above assumed bounds for UWB channel scenario parameters the limits approximation variables are as follows: $10^{-8} \le X_d \le 10^3$, $10^{-11} \le \xi_{dsub} \le 10^3$ (scale sampling of approximation domains is used).

Using (17), (18) as new variables, we can present the components of $H_A(X_d, \xi_{dsub})$ are given by (19) and (20).

$$X_{wd} = \frac{X_d}{\omega} \tag{17}$$

$$\xi_{wd} = \frac{\xi_{dsub}}{\omega} \tag{18}$$

$$H_{A1}(\omega) \approx AmpAT \cdot \sum_{k=1}^{KT_1} \frac{CT_{1(k)} \cdot {X_{wd}}^{-1}}{j\omega + AT_{1(k)} \cdot {X_{wd}}^{-1}} \tag{19}$$

$$H_{A2}(\omega) \approx AmpAF \cdot \sum_{k=1}^{KF_1} \frac{CF_{1(k)} \cdot \xi_{wd}{}^{-1}}{j\omega + AF_{1(k)} \cdot \xi_{wd}{}^{-1}} \tag{20}$$

To keep the relative error of all rational approximations under 1% for variables X_d and ξ_{dsub} we used the following number of poles (residues) in (19) and (20): KT_1=28, KF_1=40. We obtained the values of poles and residues, which are given in Tables 1 – 4. Most of the poles and residues in tables are real but some of them take the form of complex conjugate pairs. Only one value of each pair is presented in the tables. The approximations (19) and (20) are valid when the following inequalities are fulfilled (f_L and f_H are the lower and upper limits of the considered frequency band of an input signal):

$$\frac{10^{-8}}{2\pi f_L} \le X_{wd} \le \frac{10^{3}}{2\pi f_H}, \tag{21}$$

$$\frac{10^{-11}}{2\pi f_L} \le \xi_{wd} \le \frac{10^{3}}{2\pi f_H}. \tag{22}$$

We set values of f_L and f_H, as these frequencies for which the amplitude of input signal in frequency domain decreases to 2% of its maximum value.

TABLE I. POLES VALUES USED IN (20)

$AF_{1(1)}$	-6,223085189161760E-12	$AF_{1(2)}$	-4,642943424752610E-11
$AF_{1(3)}$	-2,632971537519530E-10	$AF_{1(4)}$	-1,455675152126270E-09
$AF_{1(5)}$	-7,835948594742870E-09	$AF_{1(6)}$	-4,038813536555160E-08
$AF_{1(7)}$	-1,968546136481600E-07	$AF_{1(8)}$	-9,017520026176850E-07
$AF_{1(9)}$	-3,880429205437380E-06	$AF_{1(10)}$	-1,575218154451000E-05
$AF_{1(11)}$	-6,080931050595430E-05	$AF_{1(12)}$	-2,258657597275270E-04
$AF_{1(13)}$	-8,185450184600070E-04	$AF_{1(14)}$	-2,909960541822810E-03
$AF_{1(15)}$	-4,387393681132390E-03	$AF_{1(16)}$	-9,888524748122700E-03
$AF_{1(17)}$	-3,076293295546190E-02	$AF_{1(18)}$	-5,319820485776900E-02
$AF_{1(19)}$	-8,530038238164280E-02	$AF_{1(20)}$	-2,107537360374780E-01
$AF_{1(21)}$	-4,852919518921980E-01	$AF_{1(22)}$	-1,109240947443870E+00
$AF_{1(23)}$	-2,555612087490020E+00	$AF_{1(24)}$	-5,971938758773050E+00
$AF_{1(25)}$	-1,376184845890750E+01	$AF_{1(26)}$	-3,152721189756180E+01
$AF_{1(27)}$	-7,135894598273800E+01	$AF_{1(28)}$	-1,525677339536200E+02
$AF_{1(29)}$	-3,263092485757550E+02	$AF_{1(30)}$	-7,215703463100180E+02
$AF_{1(31)}$	-1,959987932375670E+03	$AF_{1(32)}$	-1,609740959845480E+04
$Re(AF_{1(33)})$	-4,561149007155700E-01	$Im(AF_{1(33)})$	3,759847198447340E+00
$Re(AF_{1(35)})$	-2,234456627061440E-02	$Im(AF_{1(35)})$	6,279323246956080E+00
$Re(AF_{1(37)})$	-4,329006283843410E-01	$Im(AF_{1(37)})$	6,918866479018330E+00
$Re(AF_{1(39)})$	-7,023421504553170E-02	$Im(AF_{1(39)})$	7,845889264970790E+00

TABLE II. RESIDUES VALUES USED IN (20)

$CF_{1(1)}$	-7,117913128279230E-11	$CF_{1(2)}$	-2,418081305008450E-10
$CF_{1(3)}$	-1,009872969604920E-09	$CF_{1(4)}$	-4,136056787649920E-09
$CF_{1(5)}$	-1,650884157500870E-08	$CF_{1(6)}$	-6,275930275111510E-08
$CF_{1(7)}$	-2,265204113568500E-07	$CF_{1(8)}$	-7,735262801933800E-07
$CF_{1(9)}$	-2,509836311660360E-06	$CF_{1(10)}$	-7,785785657013580E-06
$CF_{1(11)}$	-2,335976441528150E-05	$CF_{1(12)}$	-6,863118137244520E-05

TABLE II RESIDUES VALUES USED IN (20) – CONT.

$CF_{1(13)}$	-2,008412931521980E-04	$CF_{1(14)}$	-5,741662909540510E-04
$CF_{1(15)}$	-5,531723198923410E-06	$CF_{1(16)}$	-1,551618675371540E-03
$CF_{1(17)}$	-3,817058019141940E-03	$CF_{1(18)}$	5,057827163347960E-05
$CF_{1(19)}$	-8,303193175562140E-03	$CF_{1(20)}$	-1,642642304640750E-02
$CF_{1(21)}$	-3,320881340611830E-02	$CF_{1(22)}$	-6,899626028833290E-02
$CF_{1(23)}$	-1,392889335153080E-01	$CF_{1(24)}$	-2,497718979548050E-01
$CF_{1(25)}$	-3,355045406579710E-01	$CF_{1(26)}$	-3,856566272181840E-01
$CF_{1(27)}$	-5,716422546437500E-01	$CF_{1(28)}$	-8,537999105459460E-01
$CF_{1(29)}$	-1,236874679092110E+00	$CF_{1(30)}$	-2,042323446540440E+00
$CF_{1(31)}$	-4,981162295862690E+00	$CF_{1(32)}$	-4,477523011713860E+01
$Re(CF_{1(33)})$	1,667279203879630E-06	$Im(CF_{1(33)})$	-2,418081305008450E-10
$Re(CF_{1(35)})$	1,604020576259050E-09	$Im(CF_{1(35)})$	-4,136056787649920E-09
$Re(CF_{1(37)})$	1,910068214302970E-06	$Im(CF_{1(37)})$	-6,275930275111510E-08
$Re(CF_{1(39)})$	8,509276835837030E-08	$Im(CF_{1(39)})$	-7,735262801933800E-07

TABLE III. POLES VALUES USED IN (19)

$AT_{1(1)}$	-3,468072678938460E+04	$AT_{1(2)}$	-4,084329133987000E+03
$AT_{1(3)}$	-4,084329133987000E+03	$AT_{1(4)}$	-1,563781940600060E+03
$AT_{1(5)}$	-1,563781940600060E+03	$AT_{1(6)}$	-8,097411700739480E+02
$AT_{1(7)}$	-8,097411700739480E+02	$AT_{1(8)}$	-4,648224593792050E+02
$AT_{1(9)}$	-4,648224593792050E+02	$AT_{1(10)}$	-2,759147884142890E+02
$AT_{1(11)}$	-2,759147884142890E+02	$AT_{1(12)}$	-1,648093132313600E+02
$AT_{1(13)}$	-1,648093132313600E+02	$AT_{1(14)}$	-9,793125301195320E+01
$AT_{1(15)}$	-9,793125301195320E+01	$AT_{1(16)}$	-5,757464436583650E+01
$AT_{1(17)}$	-5,757464436583650E+01	$AT_{1(18)}$	-3,338519930673860E+01
$AT_{1(19)}$	-3,338519930673860E+01	$AT_{1(20)}$	-1,905323688992640E+01
$AT_{1(21)}$	-1,905323688992640E+01	$AT_{1(22)}$	-1,068970034420490E+01
$AT_{1(23)}$	-1,068970034420490E+01	$AT_{1(24)}$	-5,903041999379620E+00
$AT_{1(25)}$	-5,903041999379620E+00	$AT_{1(26)}$	-3,236447835934380E+00
$AT_{1(27)}$	-3,236447835934380E+00	$AT_{1(28)}$	-1,771228217479420E+00

TABLE IV. RESIDUES VALUES USED IN (19)

$CT_{1(1)}$	2,350146540529970E+02	$CT_{1(2)}$	2,569344209997450E+01
$CT_{1(3)}$	9,518831670509370E+00	$CT_{1(4)}$	5,338428179924050E+00
$CT_{1(5)}$	3,652148004144690E+00	$CT_{1(6)}$	2,731594346342210E+00
$CT_{1(7)}$	2,117862278643390E+00	$CT_{1(8)}$	1,662991063684240E+00
$CT_{1(9)}$	1,310175845384090E+00	$CT_{1(10)}$	1,032363118014490E+00
$CT_{1(11)}$	8,136967576006300E-01	$CT_{1(12)}$	6,444822217608520E-01
$CT_{1(13)}$	5,216859836779230E-01	$CT_{1(14)}$	4,298176301264680E-01
$CT_{1(15)}$	3,251647623711980E-01	$CT_{1(16)}$	2,059919331198440E-01
$CT_{1(17)}$	1,083976847120910E-01	$CT_{1(18)}$	4,869482665415000E-02
$CT_{1(19)}$	1,918760674134540E-02	$CT_{1(20)}$	6,739120060706360E-03
$CT_{1(21)}$	2,117205644374970E-03	$CT_{1(22)}$	5,899097160435170E-04
$CT_{1(23)}$	1,427686795509540E-04	$CT_{1(24)}$	2,894938775797240E-05
$CT_{1(25)}$	4,639272389233180E-06	$CT_{1(26)}$	5,321749855904010E-07
$CT_{1(27)}$	3,637819135849780E-08	$CT_{1(28)}$	9,541742623624040E-10

IV. SPICE SIMULATOR MODELING

As a result of the approximation, described in the previous section, we obtain two transfer functions: $H_{A1}(s)$, $H_{A2}(s)$ ($j\omega = s$), as a finite series of partial fractions. The single fraction, or a couple of complex conjugate fractions, represents a partial transfer function of the two-ports, which are next used to build the subcircuits corresponding to each partial transfer function. The transfer function of the two possible two-ports has one of the following forms:

$$H_{1(k)}(s) = \frac{R_k}{s + p_k},$$
$$H_{2(k)}(s) = \frac{R_k}{s + p_k} + \frac{R_k^*}{s + p_k^*} = \frac{b_{1k}s + b_{0k}}{s^2 + a_{1k}s + a_{0k}}. \quad (23)$$

The two-ports corresponding to transfer functions $H_{1(k)}(s)$, $H_{2(k)}(s)$ are shown in Fig. 2. a, b. The values of the circuit parameters are determined by the poles and the residues, which are fixed, and by the geometry of the channel scenario.

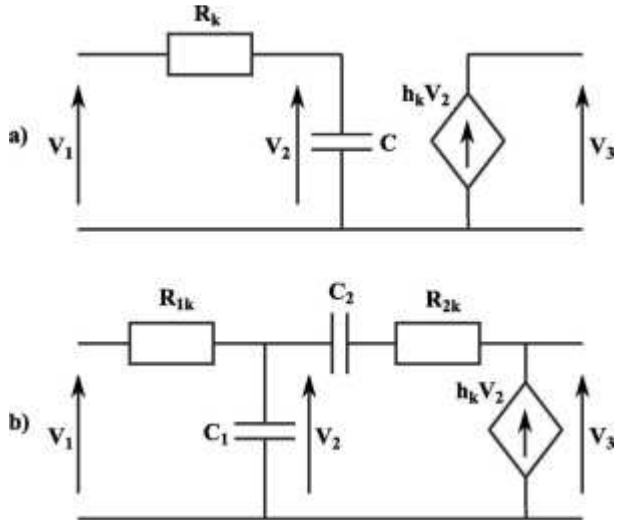

Fig. 2. Two-ports corresponding to: $H_{1(k)}(s)$-a), $H_{2(k)}(s)$-b).

Parameters R_k and p_k in (25) depend not only on residues and poles but also on geometrical parameters of a given obstacle (e.g. $R_k = CT_{1(k)} \cdot X_{wd}{}^{-1}$ and $p_k = AT_{1(k)} \cdot X_{wd}{}^{-1}$ in (19)). Assuming that parameters R_k and p_k are known, we can calculate the value of circuit elements in Fig.2. a, b in the following way:

$$C = C_0 = 10\text{pF}, \quad R_k = \frac{1}{C_0 p_k}, \quad h_k = \frac{R_k}{p_k} \quad \text{a)} \quad (24)$$

$$R_{2k}C_1 = 1, \; h_k = b_{1k}, \; \frac{h_k}{C_2} = b_{0k},$$
$$\frac{R_{2k}}{R_{1k}} + \frac{C_2}{C_1} = a_{1k}, \frac{1}{R_{1k}C_2} + 1 - h_k = a_{0k}. \quad \text{b)} \quad (25)$$

We choose arbitrarily $C_0 = 10$pF. To obtain a circuit equivalent to each ray we need also to connect an adder, an amplifier, corresponding to spreading factor A^C and a transmission line, corresponding to delay expression $exp\left(-s \cdot \frac{s^p}{V_0}\right)$ in the way resulting from (1) and (2).

V. NUMERICAL EXAMPLES

In this section we verify the results presented in Sections III and IV through simulations of TM polarized EM wave propagating on single convex obstacle. We present two numerical examples. As an input signal we use an UWB pulse given by (26) with t_c=1ns and a=0.2ns:

$$p(t) = \left(1 - 4\pi\left(\frac{t-t_c}{a}\right)^2\right) \times exp\left(-2\pi\left(\frac{t-t_c}{a}\right)^2\right), \quad (26)$$

The geometrical parameters of the scenario for the first and the second example are shown in Fig. 3 and Fig. 6, respectively. In the first example one of the creeping rays travels an obstacle along a very short distance while in the second example a creeping ray travels back into the lit region. For each example we give the ranges of frequency dependent variables X_d, X_Z, ξ_{dsub}. We use the upper index to indicate the ray to which the range corresponds. The values of frequencies f_L and f_H are 0.32 GHz and 10.40 GHz, respectively. The results of calculations for the first and the second scenario are presented in Fig. 4 and Fig. 5 – 6, respectively. In these figures, the solid line waveforms are calculated by IFFT of exact expressions (3), (10), while the dotted line waveforms are calculated directly in the time domain.

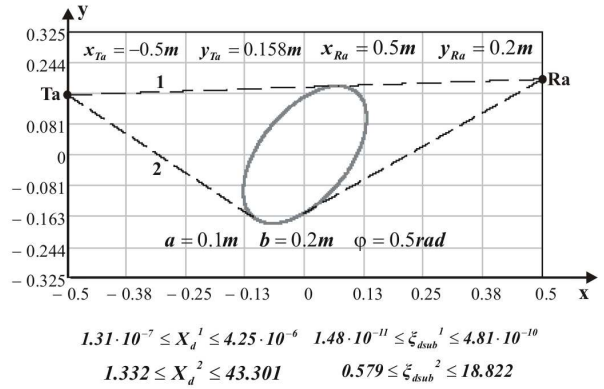

Fig. 3. The scenario of diffration rays creeping on elliptical cylinder with a "grazing incidence" case included.

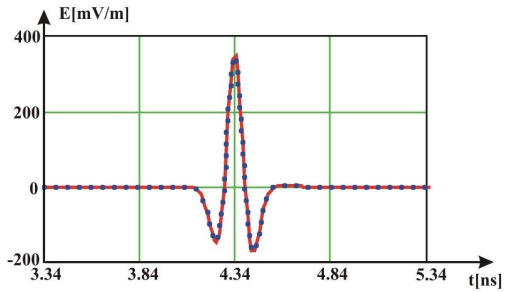

Fig. 4. The distorted UWB signal given by (26) distorted along ray no 1 from scenario shown in Fig. 3.

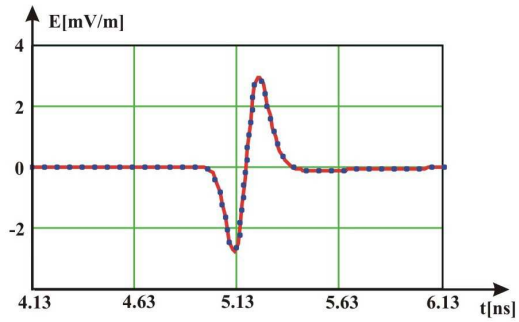

Fig. 5. The distorted UWB signal given by (26) distorted along ray no 2 from scenario shown in Fig. 3.

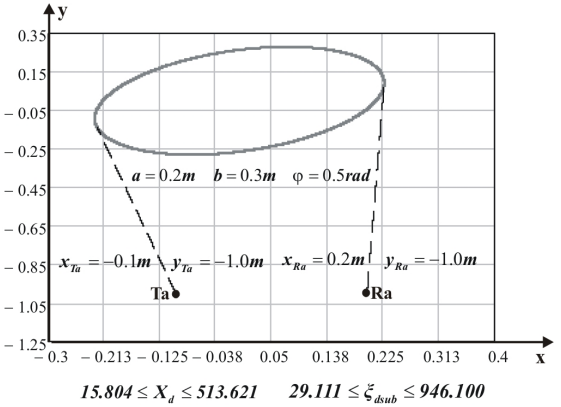

Fig. 6. The scenario of diffration ray backscattered into the lit region along elliptical cylinder.

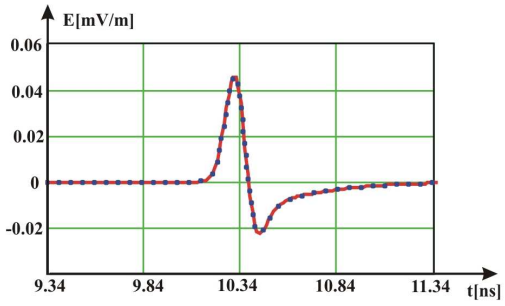

Fig. 7. The distorted UWB signal given by (26) distorted along creeping ray shown in Fig. 6.

In all examples we can see that IFFT and SPICE simulation results are in very good agreement when the ranges of X_d, ξ_{dsub} for given ray scenarios fit in the limits given in Section III.

VI. CONCLUSIONS

In the paper we presented a universal rational approximation of the transfer function of the creeping ray for the case of UWB channels containing convex obstacles. The approximation is performed using the vector fitting algorithm, which is independent of the geometry of objects in the cascade and of the frequency band (of course within reasonable limits). In order to obtain the universal vector fitting approximation we introduced the new variables. We specified the ranges of these new variables (VF approximation domain limits) that reflect the practical values of the UWB channel parameters. The new approximated transfer functions have the form of a finite series of partial fractions. All the poles and residues of the transfer functions for the TM polarization case are given in the paper. Various considered scenarios of the channel and various frequency bands can be modeled by using given poles and residues by controlling only the geometrical parameters of the scenarios (R_{el}, θ_{el} etc.).

The presented impulse response of a creeping ray has a very simple form, given by a sum of exponential functions. Therefore the obtained results are suitable for modeling an UWB channel containing a cascade of convex obstacles in SPICE-like simulators. We give examples of such modeling. The great advantage of modeling in SPICE is the possibility of including detailed models of transmitter and receiver that consider their nonlinearities. Moreover in simulations of EM wave propagation we can implement very fast and effective convolution algorithms with any input signal [10]. If the incident UWB pulse is defined by the sum of exponential functions, one only needs to perform analytical calculations in order to find the shape of a signal distorted by obstacles in a channel.

REFERENCES

[1] M.Z. Win D. Porcino, W. Hirt , "Ultra-wideband radio technology: potential and challenges ahead", *IEEE Communications Magazine*, July 2003, pp. 2-11,

[2] P. R. Rousseau, P. H. Pathak, Hsi-Tseng Chou, "A time domain formulation of the uniform geometrical theory of diffraction for scattering from a smooth convex surface", *IEEE Transactions on Antennas and Propagation*, vol. 55, no. 6, June 2007, pp. 1522-1534

[3] Chenming Zhou, R. C. Qiu, "Pulse distortion caused by cylinderdiffraction and its impact on UWB communications", in *Proc. The IEEE 2006 International Conference on Ultra-Wideband*, Waltham, MA, September 2006, pp.645-650.

[4] B. Chaudhury, P.K. Chattopadhyay, D. Raju, S. Chaturvedi, "Transient Analysis of Creeping Wave Modes Using 3-D FDTD Simulation and SVD Method", *IEEE Transactions on Antennas and Propagation*, vol. 57, no. 3, March 2009, pp. 754-759

[5] K. Naishadham, J.E. Piou, "A Robust State Space Model for the Characterization of Extended Returns in Radar Target Signatures", *IEEE Transactions on Antennas and Propagation*, vol. 56, no. 6, June 2008, pp. 1742-1751

[6] B. Gustavsen, A. Semlyen, "Rational approximation of frequency domain response by vector fitting", *IEEE Transactions on Power Delivery*, vol.14, no. 3, 1999, pp. 1052-1061.

[7] P. H. Pathak, W. Burnside, R. Marhefka, "A uniform GTD analysis of the diffraction of electromagnetic waves by a smooth convex surface", *IEEE Transactions on Antennas and Propagation*, vol. 28, no. 5, September 1980, pp. 631-642.

[8] P. Górniak, W. Bandurski, "Direct Time Domain Analysis of an UWB Pulse Distortion by Convex Objects with the Slope Diffraction Included", *IEEE Transactions on Antennas and Propagation*, vol. 56, no. 9, September 2008, pp. 3036–3044

[9] M. Ghaddar, L. Talbi, T. A. Denidni, A. Sebak, "A Conducting Cylinder for Modeling Human Body Presence in Indoor Propagation channel", *IEEE Transactions on Antennas and Propagation*, vol. 55, no. 11, November 2007, pp. 3099-3103

[10] W. Janke, G. Blakiewicz, "Semi Analytical Recursive Algorithms for Convolution Calculations", in *Proc. IEE - Circuits, Devices and Systems*, vol. 142, no. 2, April 1995, pp. 125-130